*Inorg. Chem.* **2002**, *41*, 521–531


# Sterically Hindered Carboxylate Ligands Support Water-Bridged Dimetallic Centers That Model Features of Metallohydrolase Active Sites

**Dongwhan Lee, Pei-Lin Hung, Bernhard Spingler, and Stephen J. Lippard***

*Department of Chemistry, Massachusetts Institute of Technology, Cambridge, Massachusetts 02139*

Received July 12, 2001

The synthesis and characterization of carboxylate-bridged dimetallic complexes are described. By using *m*-terphenyl-derived carboxylate ligands, a series of dicobalt(II), dicobalt(III), dinickel(II), and dizinc(II) complexes were synthesized. The compounds are $[Co_2(\mu\text{-}O_2CAr^{Tol})_2(O_2CAr^{Tol})_2L_2]$ (**1**), $[Co_2(\mu\text{-}OH_2)_2(\mu\text{-}O_2CAr^{Tol})_2(O_2CAr^{Tol})_2L_2]$ (**2a**–**c**), $[Co_2(\mu\text{-}OH)_2(\mu\text{-}O_2CAr^{Tol})_2(O_2CAr^{Tol})_2L_2]$ (**3**), $[Ni_2(\mu\text{-}O_2CAr^{Tol})_4L_2]$ (**4**), $[Ni_2(\mu\text{-}HO\cdots H)_2(\mu\text{-}O_2CAr^{Tol})_2(O_2CAr^{Tol})_2L_2]$ (**5**), and $[Zn_2(\mu\text{-}O_2CAr^{Tol})_2(O_2CAr^{Tol})_2L_2]$ (**6**), where $Ar^{Tol}CO_2H$ = 2,6-di(*p*-tolyl)benzoic acid and L = pyridine, THF, or *N,N*-dibenzylethylenediamine. Structural analysis of these complexes revealed that additional bridging ligands can be readily accommodated within the $\{M_2(\mu\text{-}O_2CAr^{Tol})_2\}^{2+}$ core, allowing a wide distribution of M···M distances from 2.5745(6) to 4.0169(9) Å. Unprecedented bridging units $\{M_2(\mu\text{-}OH_2)_2(\mu\text{-}O_2CR)_2\}^{n+}$ and $\{M_2(\mu\text{-}HO\cdots H)_2(\mu\text{-}O_2CR)_2\}^{n+}$ were identified in **2a**–**c** and **5**, respectively, in which strong hydrogen bonding accommodates shifts of protons from bridging water molecules toward the dangling oxygen atoms of terminal monodentate carboxylate groups. Such a proton shift along the O···H···O coordinate attenuates the donor ability of the anionic carboxylate ligand, which can translate into increased Lewis acidity at the metal centers. Such double activation of bridging water molecules by a Lewis acidic metal center and a metal-bound general base may facilitate the reactivity of metallohydrolases such as methionine aminopeptidase (MAP).

## Introduction

A structural motif comprising two metal ions supported by four carboxylate and one or two histidine residues is commonly encountered at metalloenzyme active sites.[1,2] Widely differing organic transformations can be catalyzed at these centers by various metal ions having a seemingly identical chemical architecture. The nature of these transformations has been a topic of great interest. The preorganized dinucleating carboxylate ligand, XDK,[3,4] and its derivatives[5,6] have been extensively used in our laboratory to model features of such enzyme active sites. Discrete dimetallic cores are stabilized by the convergent doubly bridging carboxylate platform afforded by the XDK ligand family and shielded against unwanted oligomerization reactions. Dimetallic XDK complexes of both redox-active[5−11] and -inactive[12−16] metal ions have afforded valuable structural and/or functional models for their biological counterparts, providing insights into the underlying chemical principles of metalloenzyme action.

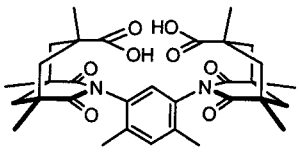


$H_2XDK$

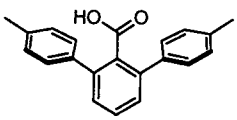


$Ar^{Tol}CO_2H$

Recently we[17−20] and others[21] demonstrated that conformationally well-defined, *m*-terphenyl-derived carboxylate

* Author to whom correspondence should be addressed. E-mail: lippard@lippard.mit.edu.

(1) Lippard, S. J.; Berg, J. M. *Principles of Bioinorganic Chemistry*; University Science Books: Mill Valley, CA, 1994.
(2) Holm, R. H.; Kennepohl, P.; Solomon, E. I. *Chem. Rev.* **1996**, *96*, 2239−2314.
(3) Abbreviations: $H_2$XDK, *m*-xylenediamine bis(Kemp's triacid imide); $Ar^{Tol}CO_2H$, 2,6-di(*p*-tolyl)benzoic acid; $Me_3$TACN, 1,4,7-trimethyl-1,4,7-triazacyclononane.
(4) Rebek, J., Jr.; Marshall, L.; Wolak, R.; Parris, K.; Killoran, M.; Askew, B.; Nemeth, D.; Islam, N. *J. Am. Chem. Soc.* **1985**, *107*, 7476−7481.
(5) Herold, S.; Lippard, S. J. *J. Am. Chem. Soc.* **1997**, *119*, 145−156.
(6) LeCloux, D. D.; Lippard, S. J. *Inorg. Chem.* **1997**, *36*, 4035−4046.
(7) Watton, S. P.; Masschelein, A.; Rebek, J., Jr.; Lippard, S. J. *J. Am. Chem. Soc.* **1994**, *116*, 5196−5205.
(8) Herold, S.; Pence, L. E.; Lippard, S. J. *J. Am. Chem. Soc.* **1995**, *117*, 6134−6135.
(9) LeCloux, D. D.; Barrios, A. M.; Mizoguchi, T. J.; Lippard, S. J. *J. Am. Chem. Soc.* **1998**, *120*, 9001−9014.
(10) LeCloux, D. D.; Davydov, R.; Lippard, S. J. *J. Am. Chem. Soc.* **1998**, *120*, 6810−6811.
(11) LeCloux, D. D.; Davydov, R.; Lippard, S. J. *Inorg. Chem.* **1998**, *37*, 6814−6826.

10.1021/ic0107431 CCC: $22.00 
Published on Web 01/10/2002

ligands can be used to assemble diiron(II) complexes that bear a close structural and functional resemblance to the active sites of selected non-heme diiron enzymes. Control over the nuclearity and coordination geometry was achieved by the interlocking nature of the flanking aryl substituents on the benzoate ligands in the complexes. The occurrence of structurally related dimetallic centers in selected metallohydrolases[22,23] prompted us to synthesize analogous tetracarboxylate dinuclear complexes and to compare their structures with those in the biological systems.

In this paper, we describe the synthesis and the structural and physical characterization of dicobalt, dinickel, and dizinc complexes coordinated by $Ar^{Tol}CO_2^-$ ligands.[3] Quadruply bridged dimetallic cores having unprecedented coordination geometries were readily obtained through efficient self-assembly from simple starting materials. From X-ray structural studies of $[Co_2(\mu\text{-}OH_2)_2(\mu\text{-}O_2CAr^{Tol})_2(O_2CAr^{Tol})_2(C_5H_5N)_2]$ (**2a**) and $[Ni_2(\mu\text{-}HO\cdots H)_2(\mu\text{-}O_2CAr^{Tol})_2(O_2CAr^{Tol})_2(C_5H_5N)_2]$ (**5**) we could observe a shift of protons on bridging water molecules toward metal-bound carboxylate groups, a process that may be relevant to a key step in the mechanism of metallohydrolases.

## Experimental Section

**General Procedures and Methods.** 2,6-Di(*p*-tolyl)benzoic acid, $Ar^{Tol}CO_2H$,[24,25] and *N*,*N*-dibenzylethylenediamine, *N*,*N*-$Bn_2$en,[26,27] were synthesized according to literature procedures. All other reagents were obtained from commercial suppliers and used as received unless otherwise noted. The reactions of $MX_2$ ($MX_2$ = $CoI_2$ or $NiBr_2$), AgOTf, $NaO_2CAr^{Tol}$, and pyridine were carried out under nitrogen in a Vacuum Atmospheres drybox. Solvents used in the drybox were purified by the following methods. Dichloromethane was distilled over $CaH_2$ under nitrogen, and diethyl ether and THF were saturated with nitrogen and purified by passage through activated $Al_2O_3$ columns under nitrogen.[28] FT-IR spectra were recorded on a Bio Rad FTS-135 instrument with Win-IR software. UV−vis spectra were recorded on a Hewlett Packard 8453 diode array spectrophotometer.

**$[Co_2(\mu\text{-}O_2CAr^{Tol})_2(O_2CAr^{Tol})_2(C_5H_5N)_2]$ (1). Method A.** To a rapidly stirred green THF (10 mL) solution of $CoI_2$ (79 mg, 0.25 mmol) was added AgOTf (142 mg, 0.55 mmol) to afford an orange suspension. A portion of $NaO_2CAr^{Tol}$ (165 mg, 0.509 mmol) was added. The heterogeneous mixture was treated with pyridine (21 $\mu$L, 0.26 mmol) and stirred overnight. Insoluble fractions were filtered off, and the deep blue filtrate was concentrated under reduced pressure. The residual blue solid was extracted into $CH_2Cl_2$ (5 mL), and insoluble material was filtered off. Vapor diffusion of ether into the filtrate afforded dark blue needles of **1** (102 mg, 68.8 $\mu$mol, 55%). Single crystals suitable for X-ray crystallography were obtained by vapor diffusion of pentanes into a concentrated solution of **1** in $CH_2Cl_2$/1,2-dichloroethane (4:1).

**Method B.** To a rapidly stirred pink THF (10 mL) solution of $Co(NO_3)_2\cdot 6H_2O$ (148 mg, 0.509 mmol) was added $Ar^{Tol}CO_2H$ (295 mg, 0.976 mmol). A portion of triethylamine (155 $\mu$L, 1.11 mmol) was added, and the blue-purple solution was treated with pyridine (41 $\mu$L, 0.51 mmol). The deep blue solution was stirred for 2.5 h and concentrated under reduced pressure. The residual dark blue oil was taken into $CH_2Cl_2$ (4 mL) and filtered. Vapor diffusion of ether into the filtrate afforded blue crystals of **1** (344 mg, 0.232 mmol, 95%) along with colorless needles, which were readily removed by washing with MeCN. FTIR (KBr, $cm^{-1}$): 3054, 3023, 2917, 2860, 1606, 1515, 1489, 1455, 1448, 1415, 1365, 1305, 1070, 1043, 852, 817, 802, 785, 759, 736, 713, 696, 545, 522. UV−vis ($CH_2Cl_2$) ($\lambda_{max}$, nm ($\epsilon$, $M^{-1}cm^{-1}$)): 540 (304), 570 (330), 590 (316), 1100 (40). Anal. Calcd for $C_{94}H_{78}N_2O_8Co_2$: C, 76.21; H, 5.31; N, 1.89. Found: C, 75.98; H, 5.53; N, 1.85.

**$[Co_2(\mu\text{-}OH_2)_2(\mu\text{-}O_2CAr^{Tol})_2(O_2CAr^{Tol})_2(C_5H_5N)_2]$ (2a).** This compound was obtained by vapor diffusion of pentanes into an aqueous $CH_2Cl_2$/acetone solution of **1**. A mixture of acetone/$H_2O$ (2:1, 3 mL) was added to a $CH_2Cl_2$ (3 mL) solution of **1** (103 mg, 69.5 $\mu$mol), inducing a color change from dark blue to pale pink. The organic layer was separated by filtration through Celite. Red purple blocks of **2** (44 mg, 26 $\mu$mol, 37%) suitable for X-ray crystallography were obtained by vapor diffusion of pentanes into the filtrate at room temperature. Upon heating in vacuo at 60 °C overnight, the crystals readily lose coordinated $H_2O$ and lattice solvent molecules, converting to a dark blue solid of **1** as determined by elemental analysis and FTIR. FTIR (KBr, $cm^{-1}$): 3549, 3053, 3024, 2919, 2863, 1589, 1515, 1487, 1450, 1407, 1381, 1307, 1265, 1218, 1187, 1150, 1110, 1070, 1042, 1020, 833, 819, 804, 787, 767, 759, 736, 699, 585, 548, 530. UV−vis ($CH_2Cl_2$) ($\lambda_{max}$, nm ($\epsilon$, $M^{-1}cm^{-1}$)): 520 (60), 550 (69), 588 (64). Anal. Calcd for $C_{94}H_{82}N_2O_{10}Co_2\cdot 2CH_2Cl_2$: C, 68.33; H, 5.14; N, 1.66. Found: C, 68.39; H, 5.24; N, 1.66.

**$[Co_2(\mu\text{-}OH_2)_2(\mu\text{-}O_2CAr^{Tol})_2(O_2CAr^{Tol})_2(THF)_2]$ (2b) and $[Co_2(\mu\text{-}OH_2)_2(\mu\text{-}O_2CAr^{Tol})_2(O_2CAr^{Tol})_2(N,N\text{-}Bn_2en)_2]$ (2c).** These compounds were obtained in a manner similar to that described for **1** except that THF or *N*,*N*-dibenzylethylenediamine (*N*,*N*-$Bn_2$en) was used instead of pyridine. Violet blocks of **2b** (34%) suitable for X-ray crystallography were obtained by recrystallization from $CH_2Cl_2/H_2O$/pentanes. Purple blocks of **2c** (64%) were obtained by recrystallization from $CH_2Cl_2/H_2O/Et_2O$ and analyzed by X-ray crystallography.

**$[Co_2(\mu\text{-}OH)_2(\mu\text{-}O_2CAr^{Tol})_2(O_2CAr^{Tol})_2(C_5H_5N)_2]$ (3).** A dark blue $CH_2Cl_2$ (4 mL) solution of **1** (238 mg, 161 $\mu$mol) was treated with $H_2O_2$ (30% aqueous, 0.5 mL) to afford a dark brown solution. The organic layer was separated by filtration through Celite. Vapor diffusion of $Et_2O$ into the filtrate afforded dark brown blocks of **3**


(12) Yun, J. W.; Tanase, T.; Pence, L. E.; Lippard, S. J. *J. Am. Chem. Soc.* **1995**, *117*, 4407−4408.
(13) Yun, J. W.; Tanase, T.; Lippard, S. J. *Inorg. Chem.* **1996**, *35*, 7590−7600.
(14) Tanase, T.; Watton, S. P.; Lippard, S. J. *J. Am. Chem. Soc.* **1994**, *116*, 9401−9402.
(15) Tanase, T.; Yun, J. W.; Lippard, S. J. *Inorg. Chem.* **1996**, *35*, 3585−3594.
(16) He, C.; Lippard, S. J. *J. Am. Chem. Soc.* **1998**, *120*, 105−113.
(17) Lee, D.; Lippard, S. J. *J. Am. Chem. Soc.* **1998**, *120*, 12153−12154.
(18) Lee, D.; Du Bois, J.; Petasis, D.; Hendrich, M. P.; Krebs, C.; Huynh, B. H.; Lippard, S. J. *J. Am. Chem. Soc.* **1999**, *121*, 9893−9894.
(19) Lee, D.; Krebs, C.; Huynh, B. H.; Hendrich, M. P.; Lippard, S. J. *J. Am. Chem. Soc.* **2000**, *122*, 5000−5001.
(20) Lee, D.; Lippard, S. J. *J. Am. Chem. Soc.* **2001**, *123*, 4611−4612.
(21) (a) Hagadorn, J. R.; Que, L., Jr.; Tolman, W. B. *J. Am. Chem. Soc.* **1998**, *120*, 13531−13532. (b) Hagadorn, J. R.; Que, L., Jr.; Tolman, W. B.; Prisecaru, I.; Münck, E. *J. Am. Chem. Soc.* **1999**, *121*, 9760−9761.
(22) Wilcox, D. E. *Chem. Rev.* **1996**, *96*, 2435−2458.
(23) (a) Lipscomb, W. N.; Sträter, N. *Chem. Rev.* **1996**, *96*, 2375−2433. (b) Sträter, N.; Lipscomb, W. N.; Klabunde, T.; Krebs, B. *Angew. Chem., Int. Ed. Engl.* **1996**, *35*, 2024−2055.
(24) Du, C.-J. F.; Hart, H.; Ng, K.-K. D. *J. Org. Chem.* **1986**, *51*, 3162−3165.
(25) Saednya, A.; Hart, H. *Synthesis* **1996**, 1455−1458.
(26) Guillaume, D.; Aitken, D. J.; Husson, H.-P. *Synlett* **1991**, 747−749.
(27) Iwanami, S.; Takashima, M.; Hirata, Y.; Hasegawa, O.; Usuda, S. *J. Med. Chem.* **1981**, *24*, 1224−1230.
(28) Pangborn, A. B.; Giardello, M. A.; Grubbs, R. H.; Rosen, R. K.; Timmers, F. J. *Organometallics* **1996**, *15*, 1518−1520.

(64 mg, 42 $\mu$mol, 26%), which were suitable for X-ray crystallography. FTIR (KBr, $cm^{-1}$): 3354, 3020, 2918, 1604, 1585, 1468, 1516, 1487, 1452, 1399, 1365, 1342, 1305, 1247, 1215, 1185, 1143, 1110, 1035, 1019, 928, 840, 822, 802, 788, 764, 736, 712, 688, 655, 592, 579, 548, 530. UV−vis ($CH_2Cl_2$) ($\lambda_{max}$, nm ($\epsilon$, $M^{-1}$ $cm^{-1}$)): 610 (310). Anal. Calcd for $C_{94}H_{80}N_2O_{10}Co_2$: C, 74.50; H, 5.32; N, 1.85. Found: C, 74.39; H, 5.28; N, 1.96.

**[$Ni_2$($\mu$-$O_2CAr^{Tol}$)$_4$($C_5H_5N$)$_2$] (4).** To a rapidly stirred THF (10 mL) suspension of $NiBr_2$ (60 mg, 0.27 mmol) was added AgOTf (146 mg, 0.568 mmol). A portion of $NaO_2CAr^{Tol}$ (170 mg, 0.524 mmol) and pyridine (21 $\mu$L, 0.26 mmol) was added, and the heterogeneous mixture was stirred overnight. Insoluble material was filtered off, and the pale green filtrate was concentrated under reduced pressure. The residual green solid was extracted into $CH_2Cl_2$ (5 mL) and filtered. Vapor diffusion of pentanes into the filtrate afforded green blocks of **4** (135 mg, 91.1 $\mu$mol, 70%), which were suitable for X-ray crystallography. FTIR (KBr, $cm^{-1}$): 3051, 3021, 2918, 2863, 1620, 1584, 1550, 1514, 1487, 1449, 1404, 1385, 1072, 848, 811, 786, 762, 710, 690, 586, 527. UV−vis ($CH_2Cl_2$) ($\lambda_{max}$, nm ($\epsilon$, $M^{-1}cm^{-1}$)): 410 (230), 680 (62). Anal. Calcd for $C_{94}H_{78}N_2O_8Ni_2$: C, 76.23; H, 5.31; N, 1.89. Found: C, 76.26; H, 5.34; N, 1.83.

**[$Ni_2$($\mu$-HO···H)$_2$($\mu$-$O_2CAr^{Tol}$)$_2$($O_2CAr^{Tol}$)$_2$($C_5H_5N$)$_2$] (5).** To a rapidly stirred THF (10 mL) suspension of $Ni(NO_3)_2$·$6H_2O$ (77 mg, 0.25 mmol) and $NaO_2CAr^{Tol}$ (166 mg, 0.512 mmol) was added pyridine (20 $\mu$L, 0.25 mmol). The heterogeneous mixture was stirred overnight, and volatile fractions were removed under reduced pressure. The residual green solid was extracted into $CH_2Cl_2$ (5 mL), and insoluble material was filtered off. Vapor diffusion of pentanes into the pale green filtrate afforded green blocks of **5**·$2CH_2Cl_2$ (163 mg, 0.107 mmol, 86%), which were suitable for X-ray crystallography. FTIR (KBr, $cm^{-1}$): 3527, 3052, 3023, 2918, 2863, 1620, 1608, 1563, 1515, 1487, 1450, 1407, 1382, 1264, 1219, 1187, 1148, 1110, 1071, 1044, 1020, 824, 805, 788, 768, 736, 699, 641, 586, 547, 531. UV−vis ($CH_2Cl_2$) ($\lambda_{max}$, nm ($\epsilon$, $M^{-1}cm^{-1}$)): 400 (47), 665 (20), 1100 (10). Anal. Calcd for $C_{94}H_{82}N_2O_{10}Ni_2$·$2CH_2Cl_2$: C, 68.35; H, 5.14; N, 1.66. Found: C, 68.63; H, 5.49; N, 1.63.

**[$Zn_2$($\mu$-$O_2CAr^{Tol}$)$_2$($O_2CAr^{Tol}$)$_2$($C_5H_5N$)$_2$] (6).** To a rapidly stirred THF (15 mL) solution of $Zn(OTf)_2$ (188 mg, 0.517 mmol) were added $NaO_2CAr^{Tol}$ (336 mg, 1.04 mmol) and pyridine (45 $\mu$L, 0.56 mmol). The reaction mixture was stirred for 5 h to afford a clear colorless solution. Volatile fractions were removed under reduced pressure, and the residual white solid was extracted into $CH_2Cl_2$ (10 mL). Insoluble material was filtered off, and vapor diffusion of pentanes into the filtrate afforded **6** (210 mg, 0.141 mmol, 54%) as colorless needles. Colorless blocks suitable for X-ray crystallography were obtained by vapor diffusion of $Et_2O$ into a concentrated $CH_2Cl_2$ solution of **6** at room temperature. FTIR (KBr, $cm^{-1}$): 3053, 3025, 2920, 2865, 1605, 1568, 1515, 1489, 1451, 1405, 1372, 1307, 1221, 1187, 1148, 1110, 1070, 1045, 1021, 954, 844, 820, 802, 787, 766, 737, 707, 699, 676, 665. Anal. Calcd for $C_{94}H_{78}N_2O_8Zn_2$·$0.25CH_2Cl_2$: C, 74.69; H, 5.22; N, 1.85. Found: C, 74,53; H, 5.43; N, 1.78.

**X-ray Crystallographic Studies.** Intensity data were collected on a Bruker (formerly Siemens) CCD diffractometer with graphite-monochromated Mo K$\alpha$ radiation ($\lambda$ = 0.71073 Å), controlled by a Pentium-based PC running the SMART software package.[29] Single crystals were mounted at room temperature on the tips of quartz fibers, coated with Paratone-N oil, and cooled to 188 K under a stream of cold nitrogen maintained by a Bruker LT-2A nitrogen cryostat. Data collection and reduction protocols are described elsewhere.[30] The structures were solved by direct methods and refined on $F^2$ by using the SHELXTL software package.[31] Empirical absorption corrections were applied with SADABS,[32] part of the SHELXTL program package, and the structures were checked for higher symmetry by the PLATON program.[33] All non-hydrogen atoms were refined anisotropically unless otherwise noted. Hydrogen atoms were assigned idealized positions and given thermal parameters equivalent to either 1.5 (methyl hydrogen atoms) or 1.2 (all other hydrogen atoms) times the thermal parameter of the carbon atom to which they were attached. The hydrogen atoms associated with the bridging water molecules in **2a**−**c**, hydroxides in **3**, and water molecules in **5** were located in the difference Fourier map and refined isotropically; those associated with disordered solvent molecules were not included in the refinement. Disordered $CH_2Cl_2$ solvent molecules in the structures of **1**, **2a**, and **5** were equally distributed over two positions and refined isotropically. In the structure of **2c**, a $CH_2Cl_2$ solvent molecule was disordered over three positions and refined with 0.5, 0.4, and 0.1 occupancies. The lattice solvent molecules in the structure of **3** were modeled as partially occupied $CH_2Cl_2$ (0.25 occupancy) and $Et_2O$ (0.75 occupancy) and refined isotropically. Crystallographic information is provided in Table 1, and Figures S1−S9 (Supporting Information) display the structures with complete atom-labeling schemes.

(29) *SMART v5.05*; Bruker AXS Inc.: Madison, WI, 1998.

## Results

**Preparation and Structural Characterization of Dicobalt(II) Complexes [$Co_2$($\mu$-$O_2CAr^{Tol}$)$_2$($O_2CAr^{Tol}$)$_2$($C_5H_5N$)$_2$] (1) and [$Co_2$($\mu$-$OH_2$)$_2$($\mu$-$O_2CAr^{Tol}$)$_2$($O_2CAr^{Tol}$)$_2$$L_2$], L = $C_5H_5N$ (2a), THF (2b), and *N*,*N*-$Bn_2$en (2c).** Reaction of $Co(OTf)_2$, generated in situ, with 2 equiv of $NaO_2CAr^{Tol}$ and 1 equiv of pyridine in anhydrous THF, afforded the neutral dicobalt(II) complex **1** in modest yield. The same air-stable compound can be conveniently prepared outside the drybox by reacting $Co(NO_3)_2$·$6H_2O$, $Ar^{Tol}CO_2H$, $Et_3N$, and pyridine in a 1:2:2:1 ratio in THF (Scheme 1). Recrystallization from $CH_2Cl_2$/$Et_2O$ provided dark blue blocks of **1** in excellent yield (~95%). The crystal structure of **1** is shown in Figure 1; selected bond lengths and angles are available in Table 2. The geometry of the cobalt(II) centers in **1** is best described as distorted trigonal pyramidal with the pyridine nitrogen atom occupying an axial position. Two cobalt atoms are related by a crystallographic inversion center, and their relatively long metal···metal separation of 3.9168(7) Å is spanned by two bridging carboxylates. The remaining coordination sites are occupied by two pyridine and two terminal carboxylates.

When a $CH_2Cl_2$ solution of **1** was exposed to aqueous organic solvents, the color changed rapidly from dark blue to pale pink. Recrystallization of **1** from water-saturated $CH_2Cl_2$/acetone/pentanes afforded red purple blocks of **2a**.

(30) Feig, A. L.; Bautista, M. T.; Lippard, S. J. *Inorg. Chem.* **1996**, *35*, 6892−6898.
(31) Sheldrick, G. M. *SHELXTL v5.1: Program for the Refinement of Crystal Structures 97-2*; University of Göttingen: Göttingen, Germany, 1998.
(32) Sheldrick, G. M. *SADABS v2.03: Area-Detector Absorption Correction*; University of Göttingen: Göttingen, Germany, 1999.
(33) Spek, A. L. *PLATON, A Multipurpose Crystallographic Tool*; Utrecht University: Utrecht, The Netherlands, 1998.

**Table 1.** Summary of X-ray Crystallographic Data

| | **1**·2$CH_2Cl_2$ | **2a**·2$CH_2Cl_2$ | **3**·0.5$CH_2Cl_2$·1.5$Et_2O$ | **4**·1.5$CH_2Cl_2$ | **5**·2$CH_2Cl_2$ | **6**·2$Et_2O$ |
|---|---|---|---|---|---|---|
| formula | $Co_2C_{96}H_{78}N_2O_8Cl_4$ | $Co_2C_{96}H_{82}N_2O_{10}Cl_4$ | $Co_2C_{100.5}H_{82}N_2O_{11.5}Cl$ | $Ni_2C_{95.50}H_{81}N_2O_8Cl_3$ | $Ni_2C_{96}H_{82}N_2O_{10}Cl_4$ | $Zn_2C_{102}H_{98}N_2O_{10}$ |
| fw | 1647.26 | 1683.30 | 1654.99 | 1608.39 | 1682.86 | 1642.56 |
| space group | $P\bar{1}$ | $P2_1/n$ | $P2_1/n$ | $P\bar{1}$ | $P2_1/c$ | $P\bar{1}$ |
| *a*, Å | 10.6629(14) | 16.3156(5) | 17.6721(17) | 14.5501(17) | 11.5584(2) | 10.556(2) |
| *b*, Å | 14.5496(19) | 14.6729(5) | 13.8244(13) | 15.2644(18) | 16.0409(2) | 14.765(3) |
| *c*, Å | 14.7554(19) | 18.0830(6) | 18.1499(17) | 19.321(2) | 23.4924(3) | 15.480(3) |
| α, deg | 109.868(2) | | | 88.881(2) | | 108.470(4) |
| *β*, deg | 103.561(2) | 102.725(1) | 106.268(1) | 81.516(2) | 100.213(1) | 94.371(4) |
| *γ*, deg | 95.425(2) | | | 75.843(2) | | 108.870(4) |
| *V*, Å$^3$ | 2054.5(5) | 4222.7(2) | 4256.6(7) | 4114.8(8) | 4286.65(11) | 2122.1(7) |
| *Z* | 1 | 2 | 2 | 2 | 2 | 1 |
| $\rho_{calc}$, g/cm$^3$ | 1.331 | 1.324 | 1.291 | 1.298 | 1.304 | 1.285 |
| *T*, °C | −85 | −85 | −85 | −85 | −85 | −85 |
| $\mu$(Mo Kα), mm$^{-1}$ | 0.593 | 0.580 | 0.485 | 0.613 | 0.624 | 0.628 |
| $\theta$ limits, deg | 1.70−28.28 | 1.52−28.26 | 1.88−28.31 | 1.94−28.30 | 1.76−28.30 | 1.69−28.26 |
| total no. of data | 18501 | 26036 | 37897 | 25919 | 37509 | 13402 |
| no. of unique data | 9276 | 9650 | 10081 | 18017 | 10072 | 9346 |
| no. of params | 527 | 523 | 523 | 1017 | 544 | 523 |
| *R* (%)[a] | 4.77 | 4.88 | 5.48 | 4.95 | 6.06 | 5.08 |
| $wR_2$ (%)[b] | 12.50 | 12.53 | 12.12 | 13.19 | 13.75 | 10.30 |
| max, min peaks, e/Å$^3$ | 0.834, −0.366 | 0.771, −1.043 | 0.551, −0.439 | 0.940, −0.878 | 0.593, −0.615 | 0.499, −0.522 |

[a] $R = \sum||F_o| - |F_c||/\sum|F_o|$. [b] $wR_2 = \{\sum[w(F_o^2 - F_c^2)^2]/\sum[w(F_o^2)^2]\}^{1/2}$.

**Scheme 1**

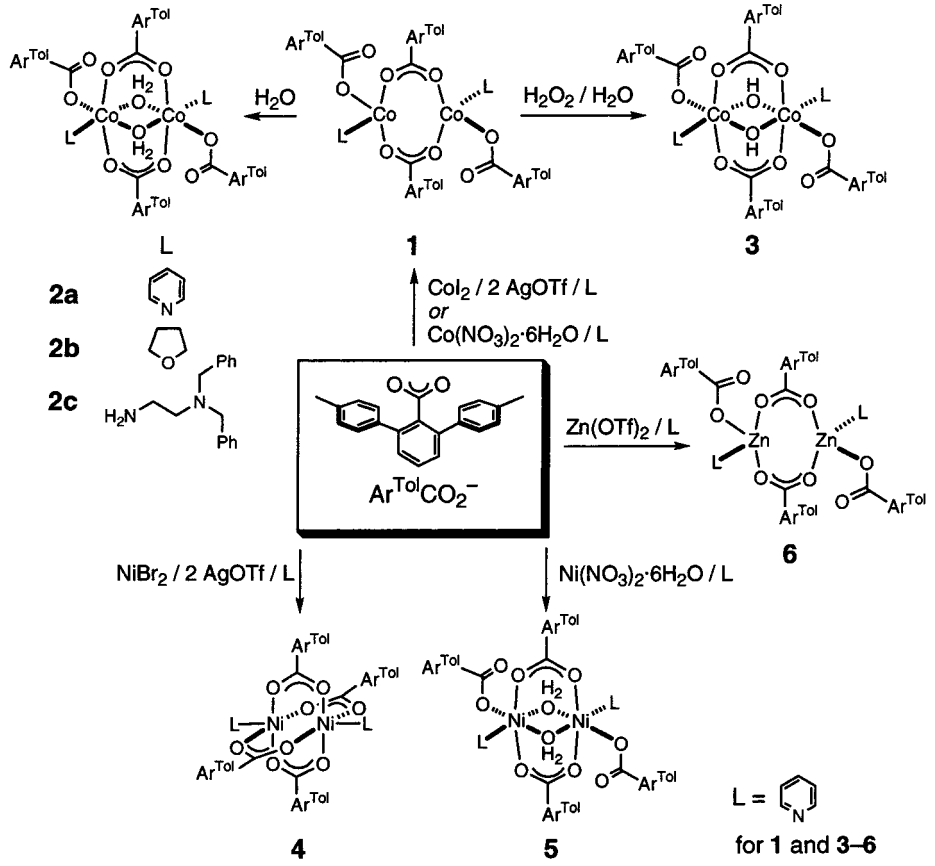


Although this material remains crystalline under ambient conditions, it turns into dark blue powders after heating at 60 °C in vacuo for >12 h. Loss of lattice solvent as well as bridging water molecules was indicated by FT-IR spectroscopy and elemental analysis, which match the properties of **1**. The crystal structure of **2a** is displayed in Figure 2; selected bond lengths and angles are listed in Table 2. In compound **2a**, two octahedral cobalt(II) centers are bridged by two $\mu$-1,3 carboxylate ligands and two water molecules. The Co···Co distance of 3.0562(6) Å is substantially (~0.86 Å) shorter than that in the precursor **1**, owing to the presence of the two bridging water molecules. The assignment of these ligands as water is supported by the Co−O distances, which range from 2.223(2) to 2.304(2) Å, as well as by the location and refinement of the associated hydrogen atoms in the X-ray structure determination (O−H, 0.74(4) and 0.86(4) Å). The two bridging carboxylate groups in **2a** are disposed trans to each other across the $\{Co_2(\mu\text{-}OH_2)_2\}^{4+}$ plane, and the two

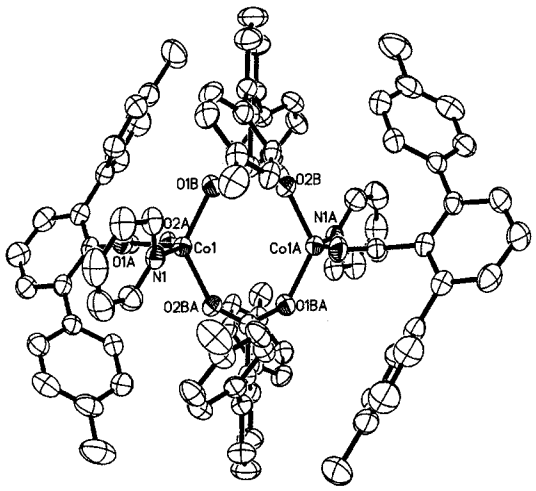


**Figure 1.** ORTEP drawing of $[Co_2(\mu\text{-}O_2CAr^{Tol})_2(O_2CAr^{Tol})_2(C_5H_5N)_2]$ (**1**) showing 50% probability thermal ellipsoids for all non-hydrogen atoms.

terminal carboxylates are hydrogen bonded to the bridging water molecules (O···O, 2.559(3) Å). Coordination of two pyridine ligands disposed *anti* across the Co−Co vector completes the pseudo-octahedral coordination sphere of each cobalt(II) center. Related dicobalt(II) complexes **2b** (Figure S1) and **2c** (Figure S2) were obtained and structurally characterized. The $\{Co_2(\mu\text{-}OH_2)_2\}^{4+}$ rhombic core structures and Co···Co distances of 3.0677(6) Å (**2b**) and 3.0521(7) Å (**2c**) are comparable to those of **2a**.

When the optimized synthetic procedure was not strictly followed, cocrystallization of **1** and **2a** occurred. Purple blocks[34] obtained from these batches revealed a disordered core structure, which was modeled as a mixture containing 75% of **1** and 25% of **2a**. The structure of **2a** overlaid on **1** (Figure S3) clearly indicates that minimal structural reorganization accompanies coordination of additional bridging water ligands. Despite geometrical variations in the dinuclear cores, the second coordination sphere structures of **1** and **2a** are essentially superimposable, suggesting that interconversion between the two compounds can readily occur by association/dissociation of water molecules.

**Preparation and Structural Characterization of $[Co_2(\mu\text{-}OH)_2(\mu\text{-}O_2CAr^{Tol})_2(O_2CAr^{Tol})_2(C_5H_5N)_2]$ (3).** Oxidation of the air-stable complex **1** with $H_2O_2$ afforded a neutral tetra(carboxylato)dicobalt(III) complex. When a $CH_2Cl_2$ solution of **1** was treated with excess aqueous $H_2O_2$, the color changed rapidly from blue to dark brown. Dark brownish green blocks of **3** were obtained after recrystallization from $CH_2Cl_2/Et_2O$ and structurally characterized. The crystal structure is shown in Figure 3; selected bond lengths and angles are reported in Table 2. The structure of the quadruply bridged dimetallic core unit, as well as the relative orientation of the terminal ligands, in **3** is close to that of the dicobalt(II) complex **2a**, although the corresponding metal−ligand bond lengths are significantly shortened due to the increased oxidation state of the metal center. Compared with the topologically related $\{Co_2(\mu\text{-}OH_2)_2\}^{4+}$ core in **2a**, the $\{Co_2(\mu\text{-}OH)_2\}^{4+}$ center in **3** has a significantly shortened Co···Co distance of 2.6802(7) Å and shorter $Co^{III}-O_{hydroxo}$ distances (1.858(2) and 1.865(2) Å). The O−M−O bite angle of the $M_2O_2$ rhombus slightly diminishes the core contraction in converting **2a** (O−Co−O = 95.10(7)°) to **3** (O−Co−O = 87.92(8)°). The terminal monodentate carboxylate groups are hydrogen bonded to the bridging ligands (O···O, 2.664(3) Å) in a manner similar to that in **2a**.

**Preparation and Structural Characterization of Dinickel(II) Complexes $[Ni_2(\mu\text{-}O_2CAr^{Tol})_4(C_5H_5N)_2]$ (4) and $[Ni_2(\mu\text{-}HO\cdots H)_2(\mu\text{-}O_2CAr^{Tol})_2(O_2CAr^{Tol})_2(C_5H_5N)_2]$ (5).** Compound **4** was synthesized by a route analogous to that used to prepare **1**. Treatment of $Ni(OTf)_2$ generated in anhydrous THF with 2 equiv of $NaO_2CAr^{Tol}$ and 1 equiv of pyridine afforded green blocks of **4** after recrystallization. The crystal structure of **4** is shown in Figure 4; selected bond lengths and angles are listed in Table 3. The metal···metal distance is 2.5745(6) Å, and there are four bridging carboxylate ligands disposed around a pseudo-$C_4$ axis along the Ni−Ni vector. The crystallographically inequivalent nickel(II) centers have similar square-pyramidal coordination geometries with average Ni−O distances of 2.019(2) Å for Ni(1) and 2.018(8) Å for Ni(2).

A reaction between $Ni(NO_3)_2\cdot 6H_2O$, $NaO_2CAr^{Tol}$, and pyridine in a 1:2:1 ratio in THF afforded green blocks of **5** after recrystallization. The structure is shown in Figure 5, and selected bond lengths and angles are reported in Table 3. The nickel(II) centers in **5** are spanned by four bridging ligands assigned as a di($\mu$-aqua)di($\mu$-carboxylato) unit. The Ni−O distances of 2.137(2) and 2.140(2) Å in the $Ni_2O_2$ rhombus fall within the range expected for partially deprotonated bridging water molecules. For comparison, the $Co-O_{aqua}$ distances in the $\{Co_2(\mu\text{-}OH_2)_2\}^{4+}$ core of **2a** are 2.223(2) and 2.304(2) Å, values significantly longer than the $Ni-O_{aqua}$ bond lengths. The metal···metal separation of 2.8923(7) Å is substantially shortened compared with that of **2a**, 3.0562(6) Å. A similar trend was observed between **2a** and **3**, for which core contraction is induced by oxidation of the metal centers as well as by deprotonation of the bridging water ligands. One hydrogen atom associated with the bridging water was located in a difference Fourier map and refined isotropically (O−H, 0.80(4) Å). The other hydrogen atom was located between the two oxygen atoms belonging to the bridging water and terminal monodentate carboxylate ligands, with $O_{aqua}-H$ and $H-O_{carboxylate}$ distances of 1.13(5) and 1.37(5) Å, respectively. The short O···O distance of 2.495(3) Å and O−H−O angle of 172(4)° indicate a strong hydrogen-bonding interaction that may facilitate formal deprotonation of the bridging water molecules.

The position of the proton between the two oxygen atoms in **5** approaches a symmetric hydrogen bond described by a single-well potential.[35] Hydrogen bonds are usually asymmetric, with the hydrogen atom located closer to the more

(34) Crystal data for **1** + **2a** (0.75:0.25): space group $P\bar{1}$ with $a$ = 10.7046(2) Å, $b$ = 14.5339(2) Å, $c$ = 14.8319(1) Å, α = 109.834(1)°, $\beta$ = 102.072(1)°, $\gamma$ = 95.894(1)°, $V$ = 2084.49(5) Å$^3$, $Z$ = 1, $R$ = 6.15%, $wR_2$ = 15.5%.

(35) (a) Hamilton, W. C.; Ibers, J. A. *Hydrogen Bonding in Solids*; Benjamin: New York, 1968. (b) Vinogradov, S. N.; Linnell, R. H. *Hydrogen Bonding*; Van Nostrand Reinhold: New York, 1971.

**Table 2.** Selected Bond Lengths (Å) and Angles (deg) for **1**·$2CH_2Cl_2$, **2a**·$2CH_2Cl_2$, and **3**·$0.5CH_2Cl_2$·$1.5Et_2O$[a]

| | bond lengths | | bond angles | |
|---|---|---|---|---|
| **1**·$2CH_2Cl_2$ | Co(1)···Co(1A) | 3.9168(7) | O(1A)−Co(1)−N(1) | 94.86(8) |
| | Co(1)−O(1A) | 1.9466(16) | O(1B)−Co(1)−O(1A) | 111.47(7) |
| | Co(1)−O(1B) | 1.9292(16) | O(1B)−Co(1)−O(2BA) | 127.65(7) |
| | Co(1)−O(2BA) | 1.9353(16) | O(1B)−Co(1)−N(1) | 101.42(8) |
| | Co(1)−N(1) | 2.049(2) | O(2BA)−Co(1)−O(1A) | 113.86(7) |
| | | | O(2BA)−Co(1)−N(1) | 99.49(8) |
| **2a**·$2CH_2Cl_2$ | Co(1)···Co(1A) | 3.0562(6) | O(1A)−Co(1)−O(1) | 83.10(7) |
| | Co(1)−O(1) | 2.3043(19) | O(1A)−Co(1)−O(1C) | 84.91(7) |
| | Co(1)−O(1C) | 2.2230(18) | O(1A)−Co(1)−N(1) | 97.16(7) |
| | Co(1)−O(1A) | 2.0220(16) | O(1B)−Co(1)−O(1A) | 102.67(7) |
| | Co(1)−O(1B) | 2.0147(16) | O(1B)−Co(1)−O(1C) | 90.24(7) |
| | Co(1)−O(2AA) | 2.0592(16) | O(1B)−Co(1)−O(2AA) | 97.31(7) |
| | O(1C)···O(2B) | 2.559(3) | O(1B)−Co(1)−N(1) | 89.63(7) |
| | O(1C)−H(1) | 0.74(4) | O(2AA)−Co(1)−N(1) | 94.91(7) |
| | O(1C)−H(2) | 0.86(4) | O(2AA)−Co(1)−O(1C) | 83.03(7) |
| | O(2B)···H(1) | 1.88(4) | O(2AA)−Co(1)−O(1) | 78.17(7) |
| | | | N(1)−Co(1)−O(1) | 84.83(7) |
| | | | O(1)−Co(1)−O(1C) | 95.10(7) |
| | | | Co(1)−O(1)−Co(1A) | 84.90(7) |
| | | | O(1C)−H(1)−O(2B) | 152(4) |
| **3**·$0.5CH_2Cl_2$·$1.5Et_2O$ | Co(1)···Co(1A) | 2.6802(7) | O(1)−Co(1)−O(1A) | 88.04(8) |
| | Co(1)−O(1) | 1.8653(17) | O(1)−Co(1)−O(1B) | 95.38(7) |
| | Co(1)−O(1C) | 1.8582(18) | O(1)−Co(1)−O(2AA) | 83.50(8) |
| | Co(1)−O(1A) | 1.9477(18) | O(1B)−Co(1)−N(1) | 85.54(8) |
| | Co(1)−O(1B) | 1.9085(17) | O(1B)−Co(1)−O(1A) | 94.09(8) |
| | Co(1)−O(2AA) | 1.9064(18) | O(1C)−Co(1)−O(2AA) | 89.58(8) |
| | Co(1)−N(1) | 1.935(2) | O(1C)−Co(1)−N(1) | 91.42(8) |
| | O(1)···O(2B) | 2.664(3) | O(1C)−Co(1)−O(1A) | 82.32(8) |
| | O(1)−H(1) | 0.89(4) | O(2AA)−Co(1)−O(1B) | 94.45(8) |
| | O(2B)···H(1) | 2.25(4) | O(2AA)−Co(1)−N(1) | 92.40(9) |
| | | | N(1)−Co(1)−O(1A) | 95.94(9) |
| | | | O(1)−Co(1)−O(1C) | 87.92(8) |
| | | | Co(1)−O(1)−Co(1A) | 92.08(7) |
| | | | O(1)−H(1)−O(2B) | 108(3) |

[a] Numbers in parentheses are estimated standard deviations of the last significant figure. Atoms are labeled as indicated in Figures 1, 2, 3, and 8.

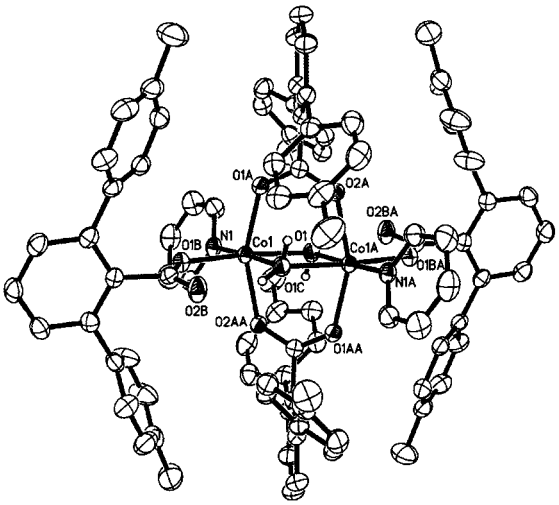


**Figure 2.** ORTEP drawing of $[Co_2(\mu\text{-}OH_2)_2(\mu\text{-}O_2CAr^{Tol})_2(O_2CAr^{Tol})_2(C_5H_5N)_2]$ (**2a**) showing 50% probability thermal ellipsoids for all non-hydrogen atoms.

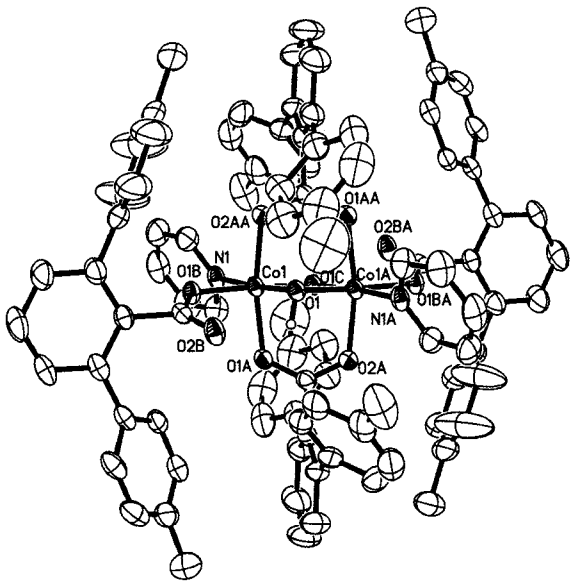


**Figure 3.** ORTEP drawing of $[Co_2(\mu\text{-}OH)_2(\mu\text{-}O_2CAr^{Tol})_2(O_2CAr^{Tol})_2(C_5H_5N)_2]$ (**3**) showing 50% probability thermal ellipsoids for all non-hydrogen atoms.

basic atom.[36] In such cases, the hydrogen atom is localized in one well of a double-well potential, a configuration favored even if the two adjacent atoms have the same basicity.[35,37] As the distance between the donors decreases, however, the barrier height is reduced and eventually disappears. At O···O distances between 2.4 and 2.5 Å, the double-well potential of O···H···O hydrogen bonds becomes a single-well having one centered hydrogen atom.[38] Although the different basicity of the two oxygen atoms may not allow an idealized O···H···O single-well potential in the HO···H···$O_2CAr^{Tol}$ unit, the strong hydrogen-bonding in-

(36) Emsley, J. *Chem. Soc. Rev.* **1980**, *9*, 91−124.
(37) Perrin, C. L.; Kim, Y.-J. *J. Am. Chem. Soc.* **1998**, *120*, 12641−12645.
(38) Peinel, G. *Chem. Phys. Lett.* **1979**, *65*, 324−326.

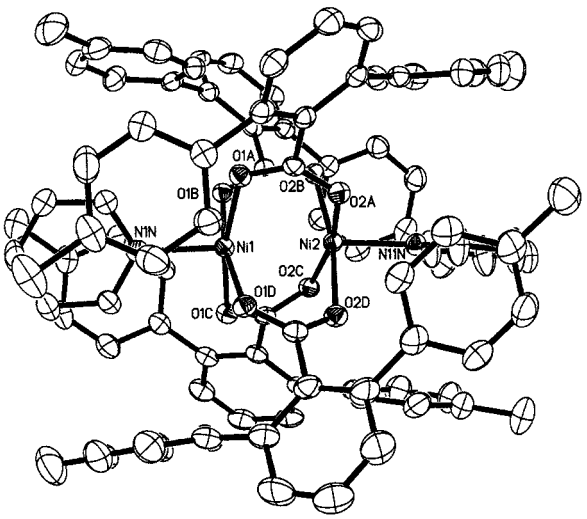


**Figure 4.** ORTEP drawing of $[Ni_2(\mu\text{-}O_2CAr^{Tol})_4(C_5H_5N)_2]$ (**4**) showing 50% probability thermal ellipsoids for all non-hydrogen atoms.

teraction apparently shifts the position of a proton toward the oxygen atom of a dangling carboxylate. A structural comparison can be made with **2a**, which has very asymmetric O···H distances of 0.74(4) and 1.88(4) Å in the HO−H···$^{-}O_2CAr^{Tol}$ unit. A longer O···O distance of 2.559(3) Å and a O−H−O angle of 152(4)° substantially deviating from linearity are consistent with weaker hydrogen bonding and a double-well potential in **2a**.

**Preparation and Structural Characterization of $[Zn_2(\mu\text{-}O_2CAr^{Tol})_2(O_2CAr^{Tol})_2(C_5H_5N)_2]$ (6).** A tetra(carboxylato)dizinc(II) complex structurally related to **1** was prepared. From a homogeneous THF solution of $Zn(OTf)_2$, $NaO_2CAr^{Tol}$, and pyridine in a 1:2:1 ratio, colorless needles of **6** crystallized in modest yield (∼54%). The structure of **6** is shown in Figure 6; selected bond lengths and angles are listed in Table 3. Two zinc(II) centers in **6** are related by a crystallographic center of inversion and bridged by two $\mu$-1,3 carboxylates. Terminal monodentate carboxylate and pyridine ligands complete the coordination spheres of tetrahedral zinc(II) sites, which are separated from each other by 4.0169(9) Å.

## Discussion

**Structures and Physical Properties.** Compounds **1** and **6** belong to a rare class of molecules in which two metal centers are bridged solely by two carboxylate ligands. This structural unit is encountered at diiron(II) centers in the active sites of the R2 subunit of ribonucleotide reductase (RNR-R2)[39] and stearoyl-ACP $\Delta^9$ desaturase ($\Delta$9D)[40] as well as the dicobalt(II) center in the active site of methionine aminopeptidase from *Escherichia coli* (EcMAP).[41] Compound **1** is only the second structurally characterized example of such a bridging unit in synthetic dicobalt(II) chemistry. The other is $[Co_2(\mu\text{-}O_2CC_6H_4CO_2H)_2(1,10\text{-phen})_4](O_2CC_6H_4CO_2H)_2$,[42] in which the two octahedral cobalt(II) centers are separated by 4.765 Å. The *syn,anti* coordination of $\mu$-1,3-bridging carboxylates expands the Co···Co distance, which is significantly longer than that (3.9168(7) Å) in **1**, which has *syn,-syn* coordination. A diiron(II) analogue of **1** and **6** having comparable geometrical parameters was previously reported.[17]

Compounds **2a**−**c** have an unprecedented ligand set connecting the two metal ions. Although triply bridged ($\mu$-aqua)di($\mu$-carboxylato)dimetallic cores have been previously observed for diiron(II),[43−47] dicobalt(II),[44,45,48,49] or dinickel(II)[50−52] complexes, a quadruply bridged di($\mu$-aqua)di($\mu$-carboxylato)dimetallic core is an unknown unit in inorganic chemistry. For edge-shared octahedral metal centers, such a bridging unit can be accommodated only by a trans disposition of the bridging carboxylate ligands across the $\{M_2(\mu\text{-}OH_2)_2\}^{n+}$ core. This requirement nicely minimizes steric interactions between the *p*-tolyl groups (Figure 2). As exemplified by **2a**−**c**, various neutral donors such as pyridine, THF, or a primary amine can coordinate the $\{Co_2(\mu\text{-}OH_2)_2(\mu\text{-}O_2CAr^{Tol})_2(O_2CAr^{Tol})_2\}$ fragment. The fact that the structure can be accommodated in a cocrystal of **1** and **2a** (Figure S3) allows us to assess the minimal degree by which uptake and loss of additional ligands requires rearrangement between the precursor and adduct. Such a structural change upon ligand association/dissociation may be relevant to the reaction cycle of metallohydrolases, for which a similarly minimal movement of protein side chains would facilitate rapid turnover. Even in the solid state, **2a** readily loses its bridging water molecules to afford the anhydrous complex **1**.

An increase in the oxidation state of a Lewis acidic metal center decreases the p$K_a$ value of coordinated water, as exemplified by the formation of the di($\mu$-hydroxo)dicobalt core upon oxidation of **2a** to **3**. Although detailed mechanistic information is not available, either outer sphere electron transfer from **2a** followed by deprotonation of bridging water molecules or O−O homolysis of a ($\mu$-1,2-hydroperoxo)-dicobalt(II) intermediate can equally well explain the formation of the di($\mu$-hydroxo)di($\mu$-carboxylato)dicobalt(III) complex **3** (Scheme 2) from **1** and aqueous $H_2O_2$. Structurally related di($\mu$-hydroxo)di($\mu$-carboxylato)diiron(III) complexes

(39) Logan, D. T.; Su, X.-D.; Åberg, A.; Regnström, K.; Hajdu, J.; Eklund, H.; Nordlund, P. *Structure* **1996**, *4*, 1053−1064.
(40) Lindqvist, Y.; Huang, W.; Schneider, G.; Shanklin, J. *EMBO J.* **1996**, *15*, 4081−4092.
(41) Roderick, S. L.; Matthews, B. W. *Biochemistry* **1993**, *32*, 3907−3912.
(42) Poleti, D.; Karanovic, L.; Bogdanovic, G. A.; Biré, A. S.-D. *Acta Crystallogr., Sect. C* **1999**, *55*, 2061−2063.
(43) Hagen, K. S.; Lachicotte, R. *J. Am. Chem. Soc.* **1992**, *114*, 8741−8742.
(44) Hagen, K. S.; Lachicotte, R.; Kitaygorodskiy, A.; Elbouadili, A. *Angew. Chem., Int. Ed. Engl.* **1993**, *32*, 1321−1324.
(45) Hagen, K. S.; Lachicotte, R.; Kitaygorodskiy, A. *J. Am. Chem. Soc.* **1993**, *115*, 12617−12618.
(46) Coucouvanis, D.; Reynolds, R. A., III; Dunham, W. R. *J. Am. Chem. Soc.* **1995**, *117*, 7570−7571.
(47) Reynolds, R. A., III; Dunham, W. R.; Coucouvanis, D. *Inorg. Chem.* **1998**, *37*, 1232−1241.
(48) Turpeinen, U.; Ahlgrén, M.; Hämäläinen, R. *Acta Crystallogr., Sect. B* **1982**, *38*, 1580−1583.
(49) Turpeinen, U.; Hämäläinen, R.; Reedijk, J. *Polyhedron* **1987**, *6*, 1603−1610.
(50) Ahlgrén, M.; Turpeinen, U. *Acta Crystallogr., Sect. B* **1982**, *38*, 276−279.
(51) Kennard, C. H. L.; O'reilly, E. J.; Smith, G. *Polyhedron* **1984**, *3*, 689−693.
(52) Eremenko, I. L.; Nefedov, S. E.; Sidorov, A. A.; Golubnichaya, M. A.; Danilov, P. V.; Ikorskii, V. N.; Shvedenkov, Y. G.; Novotortsev, V. M.; Moiseev, I. I. *Inorg. Chem.* **1999**, *38*, 3764−3773.

**Table 3.** Selected Bond Lengths (Å) and Angles (deg) for **4**·1.5$CH_2Cl_2$, **5**·2$CH_2Cl_2$, and **6**·2$Et_2O$[a]

| | bond lengths | | bond angles | |
|---|---|---|---|---|
| **4**·1.5$CH_2Cl_2$ | Ni(1)···Ni(2) | 2.5745(6) | N(1N)−Ni(1)−O(1A) | 96.90(8) |
| | Ni(1)−O(1A) | 2.0208(18) | N(1N)−Ni(1)−O(1B) | 95.89(8) |
| | Ni(1)−O(1B) | 2.0172(18) | N(1N)−Ni(1)−O(1C) | 95.10(8) |
| | Ni(1)−O(1C) | 2.0197(18) | N(1N)−Ni(1)−O(1D) | 95.79(8) |
| | Ni(1)−O(1D) | 2.0165(19) | O(1B)−Ni(1)−O(1A) | 88.20(7) |
| | Ni(1)−N(1N) | 1.994(2) | O(1B)−Ni(1)−O(1C) | 90.55(7) |
| | Ni(2)−O(2A) | 2.0090(18) | O(1D)−Ni(1)−O(1A) | 91.53(7) |
| | Ni(2)−O(2B) | 2.0250(18) | O(1D)−Ni(1)−O(1C) | 87.27(7) |
| | Ni(2)−O(2C) | 2.0144(18) | N(11N)−Ni(2)−O(2A) | 97.61(8) |
| | Ni(2)−O(2D) | 2.0237(18) | N(11N)−Ni(2)−O(2B) | 97.12(8) |
| | Ni(2)−N(11N) | 1.995(2) | N(11N)−Ni(2)−O(2C) | 95.16(8) |
| | | | N(11N)−Ni(2)−O(2D) | 93.55(8) |
| | | | O(2A)−Ni(2)−O(2B) | 92.19(7) |
| | | | O(2A)−Ni(2)−O(2D) | 88.07(8) |
| | | | O(2C)−Ni(2)−O(2B) | 86.47(7) |
| | | | O(2C)−Ni(2)−O(2D) | 90.89(7) |
| **5**·2$CH_2Cl_2$ | Ni(1)···Ni(1A) | 2.8923(7) | O(2A)−Ni(1)−O(1) | 88.46(8) |
| | Ni(1)−O(1) | 2.137(2) | O(2A)−Ni(1)−O(1B) | 97.89(8) |
| | Ni(1)−O(1C) | 2.140(2) | O(2A)−Ni(1)−N(1P) | 88.57(9) |
| | Ni(1)−O(2A) | 2.018(2) | O(2A)−Ni(1)−O(2BA) | 95.44(8) |
| | Ni(1)−O(1B) | 2.024(2) | O(1B)−Ni(1)−O(1) | 86.19(8) |
| | Ni(1)−O(2BA) | 2.078(2) | O(1B)−Ni(1)−O(1C) | 86.45(8) |
| | Ni(1)−N(1P) | 2.042(2) | O(1B)−Ni(1)−N(1P) | 96.97(9) |
| | O(1)···O(1A) | 2.495(3) | O(2BA)−Ni(1)−O(1) | 82.67(8) |
| | O(1)−H(1) | 1.13(5) | O(2BA)−Ni(1)−O(1C) | 80.95(8) |
| | O(1)−H(2) | 0.80(4) | N(1P)−Ni(1)−O(1C) | 87.87(9) |
| | O(1A)−H(1) | 1.37(5) | N(1P)−Ni(1)−O(2BA) | 94.85(9) |
| | | | O(1)−Ni(1)−O(1C) | 94.90(7) |
| | | | Ni(1)−O(1)−Ni(1A) | 85.10(7) |
| | | | O(1)−H(1)−O(1A) | 172(4) |
| **6**·2$Et_2O$ | Zn(1)···Zn(1A) | 4.0169(9) | O(1A)−Zn(1)−N(1N) | 94.74(9) |
| | Zn(1)−O(1A) | 1.973(2) | O(1B)−Zn(1)−O(1A) | 115.22(9) |
| | Zn(1)−O(1B) | 1.928(2) | O(1B)−Zn(1)−O(2BA) | 124.61(9) |
| | Zn(1)−O(2BA) | 1.9374(19) | O(1B)−Zn(1)−N(1N) | 100.28(9) |
| | Zn(1)−N(1N) | 2.061(2) | O(2BA)−Zn(1)−O(1A) | 112.50(9) |
| | | | O(2BA)−Zn(1)−N(1N) | 102.19(9) |

[a] Numbers in parentheses are estimated standard deviations of the last significant figure. Atoms are labeled as indicated in Figures 4, 5, 6, and 8.

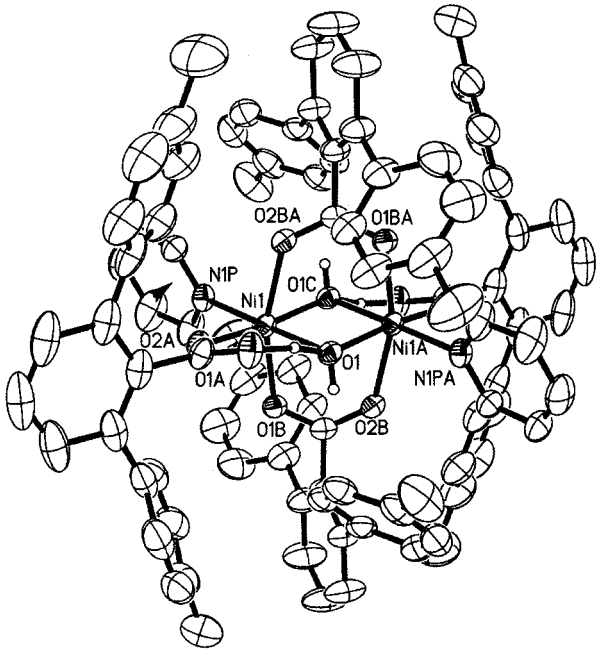


**Figure 5.** ORTEP drawing of [$Ni_2$($\mu$-HO···H)$_2$($\mu$-$O_2CAr^{Tol}$)$_2$($O_2CAr^{Tol}$)$_2$($C_5H_5N$)$_2$] (**5**) showing 50% probability thermal ellipsoids for all non-hydrogen atoms.

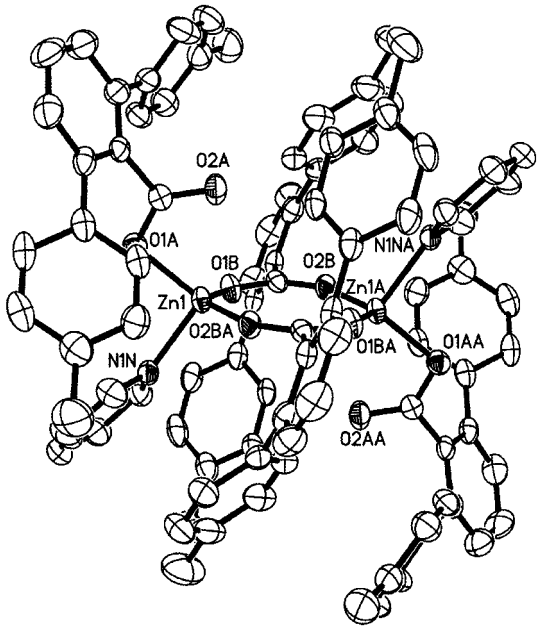


**Figure 6.** ORTEP drawing of [$Zn_2$($\mu$-$O_2CAr^{Tol}$)$_2$($O_2CAr^{Tol}$)$_2$($C_5H_5N$)$_2$] (**6**) showing 50% probability thermal ellipsoids for all non-hydrogen atoms.

were previously obtained by reactions of [$Fe_2$($\mu$-$O_2CAr^{Tol}$)$_2$($O_2CAr^{Tol}$)$_2$($C_5H_5N$)$_2$] or [$Fe_2$($\mu$-$O_2CAr^{Tol}$)$_4$(4-$^t$Bu$C_5H_4N$)$_2$] with dioxygen, which afforded [$Fe_2$($\mu$-OH)$_2$($\mu$-$O_2CAr^{Tol}$)$_2$($O_2CAr^{Tol}$)$_2L_2$] (L = $C_5H_5N$ or 4-$^t$Bu$C_5H_4N$) as isolated products.[17,18] The $Co^{III}$−$O_{hydroxo}$ distances in **3** are substantially shorter than those in the $Fe^{III}$−$O_{hydroxo}$ core (1.949(3)−2.012(2) Å)[17,18] but are comparable to $Co^{III}$−$O_{hydroxo}$

**Scheme 2**

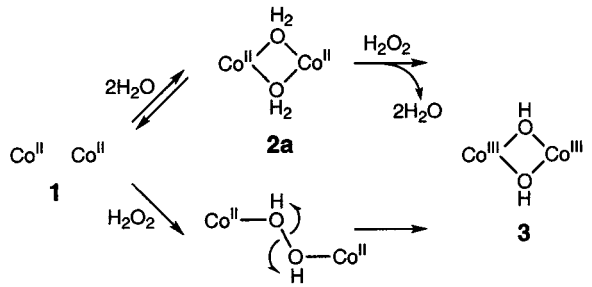

distances of ~1.90 Å for a low-spin cobalt(III) site in mixed-valence complex $[Co_2(\mu\text{-OH})(\mu\text{-OAc})_2(Me_3TACN)_2](ClO_4)_2$.[3,53] A d−d band at 610 nm ($\epsilon$ = 310 $M^{-1}$ $cm^{-1}$) is assigned to the $^1A_{1g} \rightarrow {}^1T_{1g}$ transition, by analogy to the similar 559 nm transition observed for low-spin dicobalt(III) $[Co_2(\mu\text{-OH})(\mu\text{-OAc})_2(Me_3TACN)_2](ClO_4)_3$.[53] Non-corrin mononuclear low-spin cobalt(III) centers occur in cobalt-containing nitrile hydratases that hydrolyze nitrile functional groups to afford amide products.[54] A cobalt-bound hydroxide group has been proposed as a direct nucleophile or a general base to deprotonate a water molecule that attacks the C≡N triple bonds. Metal-bound phosphodiester substrates can be attacked by a bridging oxide in dicobalt(III) complexes.[55,56] The guanidinium moiety anchored on a ($\mu$-hydroxo)dicobalt(II) core is hydrolyzed by intramolecular attack of the bridging hydroxide ion.[16]

Compound **4**, assembled under strictly anhydrous conditions, features a quadruply bridged dinickel(II) core with a short Ni···Ni distance (2.5745(6) Å). This value lies just below the range (2.603(2)−2.754(3) Å) obtained for related paddle-wheel dinickel(II) complexes.[52,57,58] For comparison, a substantially longer M···M distance of 2.8229(9) Å occurs in a diiron(II) analogue of **4**, $[Fe_2(\mu\text{-}O_2CAr^{Tol})_4(4\text{-}^tBuC_5H_4N)_2]$.[18]

Unlike the dicobalt(II) complexes **1** and **2a**, however, a dramatic structural rearrangement occurs upon incorporation of two bridging water molecules into the dimetallic core of **4**. Formal carboxylate shifts[59] of two $Ar^{Tol}CO_2^-$ ligands from $\mu$-1,3-bridging to terminal monodentate open up binding sites for additional bridging water ligands, the coordination of which is stabilized by hydrogen-bonding interaction with the terminal ligands. Structurally related dinickel(II) complexes with triply bridged $\{Ni_2(\mu\text{-OH})(\mu\text{-}O_2CR)_2\}^+$ or $\{Ni_2(\mu\text{-OH}_2)(\mu\text{-}O_2CR)_2\}^{2+}$ cores have Ni···Ni distances of 3.400(3)−3.676(3) Å, values significantly longer than the 2.8923(7) Å value in quadruply bridged **5**. The unprecedented $\{M_2(\mu\text{-HO}\cdots\text{H})_2(\mu\text{-}O_2CR)_2\}^{m+}$ bridging motif in **5** reveals

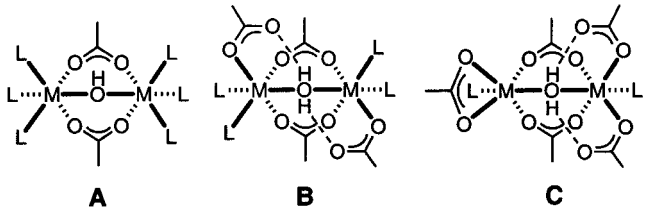

**Figure 7.** Schematic representation of carboxylate-bridged dimetallic centers having hydroxo (**A**) or aqua (**B** and **C**) bridging ligands.

"proton shifts" that can be regarded as a snapshot of an intermediate in the proton transfer step from Lewis acid-bound water to a nearby general base. This partial deprotonation of the bridging water molecules shortens the metal−oxygen bond lengths. For comparison, the Ni−O distances of 2.156(8) and 2.153(9) Å in $[Ni_2(\mu\text{-OH}_2)(\mu\text{-}O_2CCF_3)_2(O_2CCF_3)_2(tmeda)_2]$[50] are significantly longer than the 2.014(7) Å distance in $[Ni_2(\mu\text{-OH})(\mu\text{-OAc})_2(Me_3TACN)_2](ClO_4)$.[60] A similar comparison can be made between the M−O distances in the $M_2O_2$ cores of **2a** and **5**, which have $H_2O$ and HO···H bridging ligands, respectively (Tables 2 and 3). A difference in Lewis acidity at the metal center may translate into such a structural variation under identical ligand environments, although the p$K_a$ values of coordinated water in $[M(H_2O)_6]^{2+}$ are comparable for $Co^{2+}$ (9.85) and $Ni^{2+}$ (9.86) at 25 °C.[61] The p$K_a$ value of metal-bound water molecules is affected by the metal ion and its oxidation states as well as by the ancillary ligands and local dielectric.[22]

**Proton Shifts in Carboxylate-Bridged Dimetallic Centers.** A survey of structurally characterized carboxylate-bridged dicobalt(II) or dinickel(II) complexes reveals an intriguing trend between the protonation state of the bridging $H_2O/OH^-$ ligands and the composition of the ancillary ligands supporting the dimetallic core. Nitrogen-rich coordination with neutral amine/imine donors promotes the formation of ($\mu$-hydroxo)di($\mu$-carboxylato) cores (**A**, Figure 7) for cobalt(II)[53,62] or nickel(II),[60] whereas anion-rich coordination favors ($\mu$-aqua)di($\mu$-carboxylato) centers (**B** and **C**, Figure 7). Dinickel(II) compounds exclusively afford **B**.[50−52] Depending on the choice of ligands, both **B**[44,45,48,49] and **C**[46,47] are accessible for cobalt(II). In both cases, the stability of the triply bridged dimetallic centers is enhanced by the hydrogen-bonding interaction between bridging water and terminal carboxylate ligands. Even when the water molecule is bound to two metal ions, however, an anion-rich coordination environment apparently suppresses deprotonation.

Extensive studies of many enzymes have revealed carboxylate-bridged dimetallic centers at their active sites. The underlying structural and functional role of carboxylate-rich donor sets supporting such units is not fully elucidated. For example, in addition to providing structural flexibility to the dimetallic unit in the catalytic cycle, the carboxylate ligands

(53) Chaudhuri, P.; Querbach, J.; Wieghardt, K.; Nuber, B.; Weiss, J. *J. Chem. Soc., Dalton Trans.* **1990**, 271−278.
(54) Kobayashi, M.; Shimizu, S. *Eur. J. Biochem.* **1999**, *261*, 1−9.
(55) Wahnon, D.; Lebuis, A.-M.; Chin, J. *Angew. Chem., Int. Ed. Engl.* **1995**, *34*, 2412−2414.
(56) Williams, N. H.; Cheung, W.; Chin, J. *J. Am. Chem. Soc.* **1998**, *120*, 8079−8087.
(57) Hirashima, N.; Husebye, S.; Kato, M.; Maartmann-Moe, K.; Muto, Y.; Nakashima, M.; Tokii, T. *Acta Chem. Scand.* **1990**, *44*, 984−989.
(58) Morooka, M.; Ohba, S.; Nakashima, M.; Tokii, T.; Muto, Y.; Kato, M.; Steward, O. W. *Acta Crystallogr., Sect. C* **1992**, *48*, 1888−1894.
(59) Rardin, R. L.; Tolman, W. B.; Lippard, S. J. *New J. Chem.* **1991**, *15*, 417−430.
(60) Chaudhuri, P.; Küppers, H.-J.; Wieghardt, K.; Gehring, S.; Haase, W.; Nuber, B.; Weiss, J. *J. Chem. Soc., Dalton Trans.* **1988**, 1367−1370.
(61) Sillén, L. G.; Martell, A. E. *Stability Constants of Metal-Ion Complexes*; The Chemical Society: London, 1971.
(62) Lachicotte, R.; Kitaygorodskiy, A.; Hagen, K. S. *J. Am. Chem. Soc.* **1993**, *115*, 8883−8884.

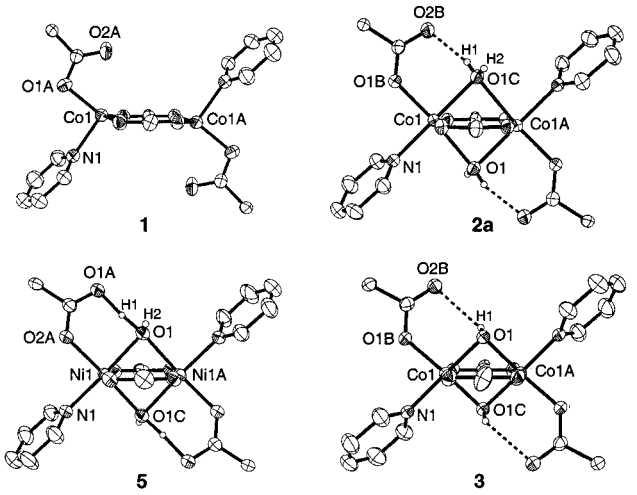


**Figure 8.** Core structures of $[Co_2(\mu\text{-}O_2CAr^{Tol})_2(O_2CAr^{Tol})_2(C_5H_5N)_2]$ (**1**), $[Co_2(\mu\text{-}OH_2)_2(\mu\text{-}O_2CAr^{Tol})_2(O_2CAr^{Tol})_2(C_5H_5N)_2]$ (**2a**), $[Ni_2(\mu\text{-}HO\cdots H)_2(\mu\text{-}O_2CAr^{Tol})_2(O_2CAr^{Tol})_2(C_5H_5N)_2]$ (**5**), and $[Co_2(\mu\text{-}OH)_2(\mu\text{-}O_2CAr^{Tol})_2\text{-}(O_2CAr^{Tol})_2(C_5H_5N)_2]$ (**3**). For clarity, all atoms of the 2,6-di(*p*-tolyl)-benzoates, except for the carboxylate groups and α-carbon atoms, were omitted.

**Scheme 3**

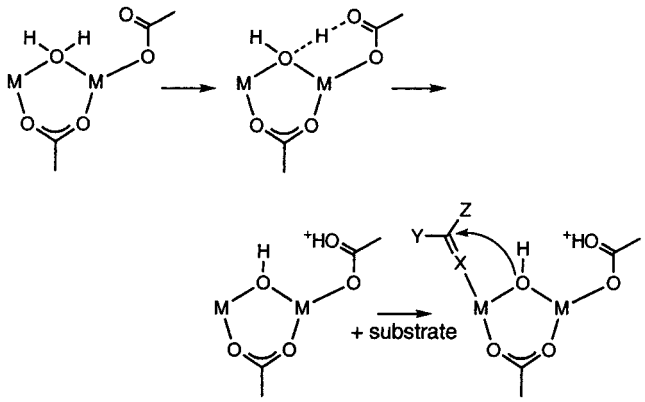


coordinating iron centers in non-heme diiron enzymes donate electrons to help cleave the O−O bond of the initial dioxygen adduct(s), enabling access to high-valent diiron(IV) species.[63−65] A similar carboxylate-rich ligand environment, however, may be a liability for metallohydrolases such as aminopeptidases or phosphohydrolases, in which the oxidation states of the low-valent metal ions do not change during catalysis. The Lewis acidity of the protein-bound metal centers would be significantly attenuated by an anion-rich first coordination sphere, rendering metal-bound nucleophiles less reactive. This situation is quite different from the histidine-rich active sites in both mononuclear and dinuclear metallohydrolases, including carboxypeptidase A, thermolysin, carbonic anhydrase, or urease.[1,22,23,66] Understanding the role of carboxylate-rich centers in this seemingly unfavorable

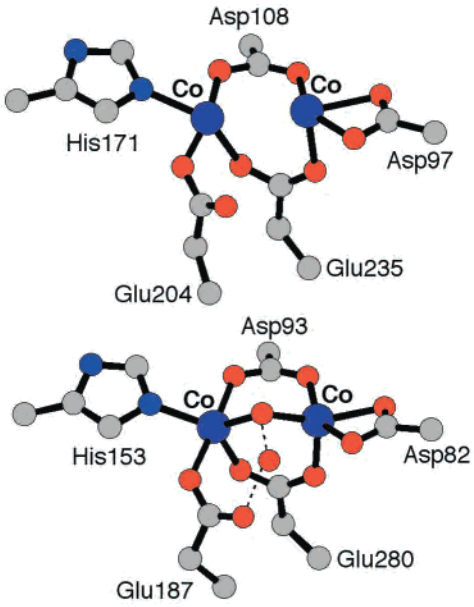


**Figure 9.** Structures of the dicobalt centers in methionine aminopeptidases from *E. coli* (EcMAP, top) and *P. furiosus* (PfMAP, bottom). Hydrogen bonds between water molecules and carboxylate residue in PfMAP are presented as broken lines. Generated from PDB files 1MAT and 1XGS, respectively.

situation can provide mechanistic insight into hydrolytic chemistry catalyzed by Lewis-acidic metal centers.

The dimetallic core structures of **1**, **2a**, **3**, and **5** provide, within an identical ancillary ligand architecture, sequential snapshots of the biomimetic activation of bridging water molecules (Figure 8). A detailed structural description is now available for the protonation states of the metal-bound water molecules and shuttling of protons between adjacent oxygen atoms. The results presented here support the notion that metal-bound carboxylate residues in enzyme active sites may act similarly as a general base to assist activation of bridging water molecules, a process facilitated by the thermodynamically favored five-membered chelate ring shown in Scheme 3. Strong hydrogen bonding with the dangling carboxylate oxygen atom helps to polarize the HO···H bonds, priming them for heterolytic cleavage to form $OH^-$ and $H^+$. The leaving proton is shuttled to the noncoordinating oxygen atom of the terminal carboxylate, thus attenuating the donor ability of this anionic ligand. Such decreased electron donation from the terminal ligand can translate into an increased Lewis acidity of the metal ion, which may be beneficial for activation of incoming electrophilic substrates. The minimal nuclear motion accompanying this process can significantly lower the kinetic barrier for fast enzymatic turnover.

**Biological Relevance: Dicobalt(II) Centers in Methionine Aminopeptidases.** Mechanistic insights gleaned from the structural analyses of small molecules described above can be used to help understand related systems in biology. Methionine aminopeptidase (MAP) is a cobalt-dependent enzyme that removes the N-terminal methionine of nascent polypeptide chains.[54] Such modification is crucial for functional regulation, intracellular targeting, and degradation of proteins. Previous structural characterization of methionine aminopeptidase from *E. coli* (EcMAP) identified four car-

(63) Solomon, E. I.; Brunold, T. C.; Davis, M. I.; Kemsley, J. N.; Lee, S.-K.; Lehnert, N.; Neese, F.; Skulan, A. J.; Yang, Y.-S.; Zhou, J. *Chem. Rev.* **2000**, *100*, 235−349.
(64) Du Bois, J.; Mizoguchi, T. J.; Lippard, S. J. *Coord. Chem. Rev.* **2000**, *200*−*202*, 443−485.
(65) Merkx, M.; Kopp, D. A.; Sazinsky, M. H.; Blazyk, J. L.; Müller, J.; Lippard, S. J. *Angew. Chem., Int. Ed.* **2001**, *40*, 2782−2807.
(66) Bertini, I.; Gray, H. B.; Lippard, S. J.; Valentine, J. S. *Bioinorganic Chemistry*; University Science Books: Mill Valley, CA, 1994.

boxylate (two Asp and two Glu) and one histidine residues surrounding the catalytic dicobalt(II) core (Figure 9).[41] A recent structural determination of a MAP from *Pyrococcus furiosus* (PfMAP) revealed structurally analogous dicobalt(II) centers in the active sites.[67] In PfMAP, two cobalt(II) ions are bridged by two carboxylate groups and one water molecule, rendering each cobalt(II) site distorted trigonal bipyramidal (Figure 9).

Comparison of the core structures of EcMAP and PfMAP indicates that a minimal structural change occurs upon incorporation of water molecules into the first coordination sphere of the dicobalt(II) core, similarly to the interconversion between **1** and **2a**. Across a second water molecule there extends a hydrogen-bonding network from the bridging water molecule to the terminally bound carboxylate group (E187) of PfMAP. Such a secondary interaction may assist deprotonation of the bridging water molecule, a process modeled by compounds **2a** and **5**. A recent structural analysis of the EcMAP protein-inhibitor complex also points toward a mechanism in which the terminal carboxylate (E204) facilitates proton transfer from the metal-bound nucleophile.[68]

## Summary and Conclusions

Discrete dicobalt(II), dicobalt(III), dinickel(II), and dizinc(II) complexes **1**−**6** have been efficiently assembled with the use of sterically hindered *m*-terphenyl-derived carboxylate ligands. Structural analyses of these complexes indicate that additional bridging ligands can be readily accommodated within the tetra(carboxylato)dimetallic unit. Unprecedented structural cores, $\{M_2(\mu\text{-}OH_2)_2(\mu\text{-}O_2CR)_2\}^{n+}$ and $\{M_2(\mu\text{-}HO\cdots H)_2(\mu\text{-}O_2CR)_2\}^{n+}$, were identified. Strong hydrogen-bonding interactions with the terminal carboxylate groups should assist deprotonation of bridging water molecules. These groups thus could be activated by the dual action of Lewis acidic metal center and metal-bound general base, a process that may be relevant to the action of selected metallohydrolases having carboxylate-bridged dinuclear centers.

**Acknowledgment.** This work was supported by a grant from the National Science Foundation. P.-L.H. acknowledges the UROP Office of MIT for financial support. B.S. was supported by the Swiss National Science Foundation as a postdoctoral fellow.

**Supporting Information Available:** Figures S1−S3 showing the ORTEP diagrams of **2b**, **2c**, and **1** + **2a** and S4−S9 displaying fully labeled ORTEP diagrams for **1**−**6**. X-ray crystallographic files, in CIF format, for complexes **1**−**6**. This material is available free of charge via the Internet at http://pubs.acs.org.

IC0107431

(67) Tahirov, T. H.; Oki, H.; Tsukihara, T.; Ogasahara, K.; Yutani, K.; Ogata, K.; Izu, Y.; Tsunasawa, S.; Kato, I. *J. Mol. Biol.* **1998**, *284*, 101−124.
(68) Lowther, W. T.; Zhang, Y.; Sampson, P. B.; Honek, J. F.; Matthews, B. W. *Biochemistry* **1999**, *38*, 14810−14819.